ORIGINAL ARTICLE

Detection and identification of cutting chatter based on improved variational nonlinear chirp mode decomposition

Jiangchuan Niu[1,2] · **Guichun Ning**[2] · **Yongjun Shen**[1,2] · **Shaopu Yang**[1,2]

Abstract

During the turning process of the lathe, the cutting chatter may be generated with the increase of cutting vibration amplitude, which is harmful to machining precision of the turning process. In order to effectively avoid the influence of cutting chatter during the turning process, the improved variational nonlinear chirp mode decomposition (VNCMD) algorithm is presented for the detection and identification of cutting chatter. The wideband and weak characteristic of the vibration signal are considered by the improved algorithm, which cannot only overcome the mode mixing and pseudo-component problems of the empirical mode decomposition (EMD) algorithm but also overcome the drawbacks of the wideband signal extraction. To eliminate the influence of uncertainty of the number of signal components on the decomposition of the VNCMD algorithm, the cross-correlation coefficient method is used to determine the optimal number of signal intrinsic mode functions. And the improved algorithm is further applied to the detection of the cutting chatter, where the fourth-order cumulant, permutation entropy, and instantaneous frequency of the signal intrinsic mode functions are extracted as the multi-feature vector for the cutting chatter. As the results show, it can effectively identify the existence and extent of cutting chatter.

Keywords Cutting chatter · VNCMD algorithm · Correlation coefficient · Permutation entropy

1 Introduction

With the demand for higher efficiency and precision in machining, the development of machine tools has encountered many problems, such as the cutting chatter caused by external interference factors or the nature of the workpiece [1]. Cutting chatter is a strong self-excited vibration that occurs between the workpiece and the cutting tool [2]. Many disadvantages may be induced by the chatter, such as the reduction of the workpiece surface finish, the damage of the cutting tool, and the decrease of cutting tool life. The common types of cutting chatter are mode coupling chatter, frictional chatter, and regenerative chatter [3–6]. In order to study chatter better, the accurate dynamical model needs to be built for the dynamic characteristics and cutting process of machine tool, but the reliability of the established model is difficult to guarantee [7, 8]. As a result, the study of cutting chatter is mainly focused on the extraction of fault features and the identification of the chatter status.

Cutting vibrations are always nonstationary and nonlinear [9, 10]. Therefore, the statistical characteristics of vibration signal in the time domain and frequency domain varied with the change of vibration, and this change is usually disturbed by the background noise. In order to better analyze the characteristic of chatter state, Choi and Shin [11] proposed the maximum likelihood estimation algorithm based on wavelet analysis. Wu and Du [12] extracted the limit cycle characteristics as an indicator of chatter state based on the wavelet transform and signal reconstruction method. Vela-Martinez et al. [13] monitored the evolution of cutter tool dynamics by using the detrended fluctuation analysis method, which is adapted for time-frequency domain. Kuljanic et al. [14, 15]

✉ Jiangchuan Niu
    menjc@163.com

    Guichun Ning
    1227374224@qq.com

    Yongjun Shen
    shenyongjun@126.com

    Shaopu Yang
    yangsp@stdu.edu.cn

1   State Key Laboratory of Mechanical Behavior and System Safety of Traffic Engineering Structures, Shijiazhuang Tiedao University, Shijiazhuang, China

2   School of Mechanical Engineering, Shijiazhuang Tiedao University, Shijiazhuang, China

proposed the wavelet analysis method based on the multiple sensor chatter monitoring system, and they used the statistical parameters obtained from wavelet decomposition to detect chatter by using an artificial intelligence classification system based on neural networks. The EMD algorithm has been applied to the signal processing of cutting chatter by a number of researchers [16–18]. Wang et al. [19] proposed a rotor fault feature detection method based on the variational mode decomposition (VMD) and achieved good results. Recently, the widespread concern has been caused by various fields' variational nonlinear chirp mode decomposition (VNCMD) algorithm proposed by Chen et al. [20]. It is because the wideband nonlinear signals with many similar modes could be decomposed from the time domain by VNCMD, which has good convergence performance even in a noisy environment.

Some new feature extraction methods have been studied when the cutting chatter characteristics are weak and difficult to extract. For example, Grabec et al. [21] extracted the chatter characteristics based on coarse-grained entropy. Berger et al. [22] proposed the chatter feature extraction method based on Toeplitz matrix singular value. Bickraj et al. [23] proposed the index-based reasoning for chatter detection and tool wear estimation by using the torque signal data of rotary dynamometers during the end milling operation. In this paper, the detection and identification of lathe cutting chatter are investigated based on the improved VNCMD algorithm. And it is organized as follows. In Section 2, the principle and improvement of VNCMD algorithm are presented. In Section 3, the improved VNCMD algorithm is verified by the simulation signals. In Section 4, the experimental signals are analyzed by the improved VNCMD algorithm. Section 5 identifies the vibration status based on multi-feature vector for the lathe cutting chatter. Finally, the main conclusions are drawn.

2 Principle and improvement of the VNCMD algorithm

2.1 Principle of the VNCMD algorithm

Huang et al. [24] believe that any signal is composed of several intrinsic mode functions (IMFs). A signal can contain several intrinsic mode functions at any time. Based on the VNCMD algorithm, the nonlinear signals can be adaptively decomposed into a series of IMFs with amplitude modulation (AM) and frequency modulation (FM) characteristics through the joint optimization scheme. The intrinsic mode functions of signal can be expressed as

$$g_i(t) = a_i(t)\cos\left[2\pi\int_0^t f_i(s)\mathrm{d}s + \phi_i\right] \tag{1}$$

where $a_i(t)$ denotes the instantaneous amplitude (IA) of the signal component, $f_i(s)$ denotes the instantaneous frequency (IF), and ϕ_i

stands for the initial phase. And the phase is $f_i(t) = 2\pi\int_0^t f_i(s)\mathrm{d}s + \phi_i$, then one could have $|a_i'(t)|$, $|f_i'(t)| << |f(s)|$ [25].

In practice, the collected signal consists of many intrinsic mode functions and the measurement noise; thus, it can be expressed as the following model

$$g(t) = \sum_{i=1}^{Q} a_i(t)\cos\left[2\pi\int_0^t f_i(s)\mathrm{d}s + \phi_i\right] + n(t) \tag{2}$$

where Q is the number of signal intrinsic mode functions which is assumed to be known, $n \sim N(0, \sigma^2)$ denotes the Gaussian white noise. According to Ref. [26], $a(t)$ can be assumed as a band-limited function, and its bandwidth can be estimated as

$$BW = BW_{\mathrm{AM}} + BW_{\mathrm{FM}} \tag{3}$$

where $BW_{\mathrm{AM}} = 2F_a$ denotes the bandwidth resulting from the AM, and F_a stands for the maximum frequency of $a(t)$. BW_{FM} is the bandwidth caused by the FM and it can be determined by the Carson bandwidth rule [27]. And $a(t)$ is a slowly varying function. For a wide-band intrinsic mode function component, its total bandwidth is often dominated by BW_{FM}, and one could have

$$BW_{\mathrm{FM}} >> BW_{\mathrm{AM}} \tag{4}$$

Next, the demodulation operator and modulation operator can be defined as [28]:

$$\Phi^-(t) = \exp\left\{-j2\pi\left[\int_0^t \overline{f}(s)\mathrm{d}s - f_c t\right]\right\} \tag{5a}$$

$$\Phi^+(t) = \exp\left\{j2\pi\left[\int_0^t \overline{f}(s)\mathrm{d}s - f_c t\right]\right\} \tag{5b}$$

where $\overline{f}(s)$ denotes the frequency function of the operators and $f_c > 0$ is a carrier frequency. According to the principle of Fourier series, smoothing function can be uniformly approximated. And the demodulated signal in Eq. (1) can be expressed as

$$g_i(t) = a_i(t)\cos\left\{2\pi\int_0^t\left[f_i(t) - \overline{f}_i(t)\right]\mathrm{d}s + \phi_i\right\}\cos\left[2\pi\int_0^t \overline{f}_i(s)\mathrm{d}s\right]$$
$$- a_i(t)\sin\left\{2\pi\int_0^t\left[f_i(s) - \overline{f}_i(s)\right]\mathrm{d}s + \phi_i\right\}\sin\left[2\pi\int_0^t \overline{f}_i(s)\mathrm{d}s\right] \tag{6}$$

According to Eqs. (5a, 5b) and (6), the signal of Eq. (2) can be obtained as

$$g(t) = \sum_{i=1}^{Q}\left\{u_i(t)\cos\left[2\pi\int_0^t \overline{f}_i(s)\mathrm{d}s\right] + v_i(t)\sin\left[2\pi\int_0^t \overline{f}_i(s)\mathrm{d}s\right]\right\} + n(t) \tag{7}$$

where $u_i(t)$ and $v_i(t)$ are two demodulated signals given as:

$$u_i(t) = a_i(t)\cos\left\{2\pi\int_0^t\left[f_i(s) - \overline{f}_i(s)\right]\mathrm{d}s + \phi_i\right\} \tag{8a}$$

$$v_i(t) = -a_i(t)\sin\left\{2\pi\int_0^t\left[f_i(s)-\overline{f}_i(s)\right]\mathrm{d}s + \phi_i\right\} \quad (8b)$$

The IA of Eq. (8a, 8b) can be expressed as

$$a_i(t) = \sqrt{u_i^2(t) + v_i^2(t)} \quad (9)$$

The square of the L$_2$ norm of the second-order derivative is used to estimate the signal bandwidth [29]. And the decomposition problem can be formulated as:

$$\min_{\{u_i\}\{v_i\}\{\overline{f}_i\}}\left\{\sum_{i=1}^{Q}\left(\left\|u_i''(t)\right\|_2^2 + \left\|v_i''(t)\right\|_2^2\right)\right\}$$

$$s.t. \left\|g(t)-\sum_i^{Q}\left(u_i(t)\cos\left[2\pi\int_0^t\overline{f}_i(s)\mathrm{d}s\right] + v_i(t)\sin\left[2\pi\int_0^t\overline{f}_i(s)\mathrm{d}s\right]\right)\right\|_2 \leq \varepsilon \quad (10)$$

where $\varepsilon > 0$ is an upper bound determined by the noise level. The optimal $\overline{f}_i(s)$ of the demodulated signals $u_i(t)$ and $v_i(t)$ can be simultaneously searched by Eq. (10). That makes the IMFs have the narrowest frequency band. Note that the difference from many methods such as the VMD is that the influence of noise is explicitly considered. Consequently, the VNCMD will have better convergence and filtering performance in noisy environment in comparison with alternative methods.

The detailed derivation process and the flow of the algorithm refer to [20, 30].

2.2 Improvement of the VNCMD algorithm

Based on the above principle of VNCMD, the decomposition results will be affected by the number of IMFs. However, the number of IMFs is uncertain in the practical signal processing. If the given number of IMFs is larger, the signals whose frequencies are concentrated in a range will be decomposed into several IMFs, which will lead to the center frequency being closer, and result in the generating of frequency aliasing components. If the given number of IMFs is smaller, some key information of the original signal will be filtered by the time-frequency filter. At this time, the decomposition components of the original signal will not be comprehensive. In order to overcome the above limitations, the number of IMFs is determined based on the cross-correlation coefficient. When the maximum center frequency of the IMFs occurs, the cross-correlation coefficients of the IMFs are calculated. The number of IMFs can be determined by analyzing whether the frequency aliasing of IMFs components is generated. The correlation coefficient for the given sequence signals x and y is defined as follows [31]:

$$\rho_{xy} = \frac{\frac{1}{N}\sum_{i=1}^{N}x(i)y(i)-E(x)E(y)}{\sqrt{\left[\frac{1}{N}\sum_{i=1}^{N}x^2(i)-E^2(x)\right]\left[\frac{1}{N}\sum_{i=1}^{N}y^2(i)-E^2(y)\right]}} \quad (11)$$

where E is the mathematical expectation, and N is the length of the sequence signals. Letting x and y be the decomposition components of the given signal, the correlation coefficients of each IMFs can be obtained by using Eq. (11).

The calculation process of the optimization algorithm is as follows:

1. The number of signal IMFs is initialized as $Q = 2$, and Q is recorded as PQ.
2. By introducing the parameter K to VNCMD, the signal components can be obtained by processing the original signal.
3. Calculating the cross-correlation coefficients between each signal components, the maximum value can be obtained.
4. The threshold is selected as 0.1 through a lot of experiments.
5. Judge whether the maximum cross-correlation coefficient exceeds the threshold; if it exceeds, the number of IMFs is determined as PQ, and the process ends.
6. If the maximum cross-correlation coefficient does not exceed the threshold, Q is recorded as PQ and the number of IMFs is set to $Q = Q + 1$, and repeat step 3.

3 Verification by simulation signals

Before the practical signal processing, the improved algorithm needs to be verified by the simulation signals. Therefore, a synthetic signal consisting of four signals is selected to analyze and verify. The simulation signal Sig can be expressed as:

$$s1 = \exp(-0.03t)\cos\left[2\pi\left(1.3 + 25t + 4t^2-0.8t^3 + 0.07t^4\right)\right]$$
$$s2 = 0.9\exp(-0.06t)\cos\left[2\pi\left(2.6 + 40t + 8t^2-1.6t^3 + 0.14t^4\right)\right]$$
$$s3 = 0.8\exp(-0.09t)\cos\left[2\pi\left(3.9 + 60t + 12t^2-2.4t^3 + 0.21t^4\right)\right] \quad (12)$$
$$\text{noise} = \text{addnoise}(\text{length}(\text{Sig}), 0, 0.5)$$
$$Sig = s1 + s2 + s3 + \text{noise}$$

As can be seen from Eq. (12), the simulation signal is composed of three AM-FM components and a Gaussian noise of power 0.5. To maintain the same conditions as the practical cutting vibration signal, the simulation signal is sampled with 12800 Hz. The time domain waveform of the simulation signal is shown in Fig. 1.

As can be seen from Fig. 1, the AM-FM signal has no obvious abrupt characteristics. That is said its bandwidth is not large. Therefore, under the interference of strong noise, the parameter *alpha* of VNCMD should be selected to be 4.8e −10, and the parameter *beta* of VNCMD should be selected to be 0.5e−10. The values of these two parameters are not fixed; they should be determined by the characteristics of the signal and require a lot of debugging. If the parameter *alpha* is larger, it can help the VNCMD algorithm to find the correct IMFs
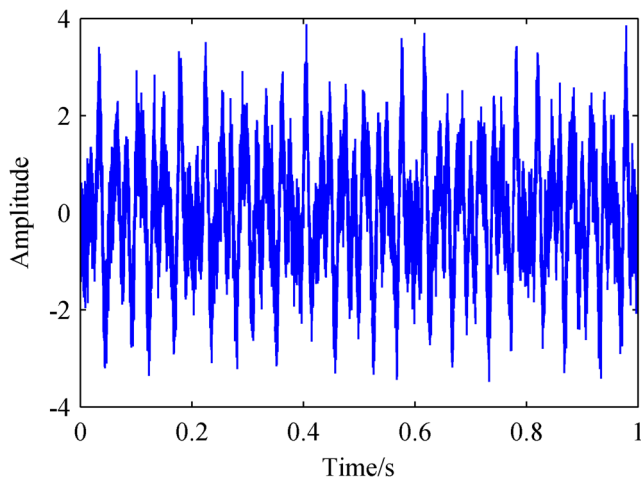
Fig. 1 Simulation signal in time domain

even if the initial instantaneous frequency is too rough. But it will introduce more noise and also may increase the interference between the signal IMFs. The parameter *beta* can be smaller which will be helpful for the convergence, but it cannot track fast varying instantaneous frequency properly. For the sake of simplicity, the initial number of IMFs is set to 3, and the signal is decomposed by the improved VNCMD algorithm. Next, the correlation coefficients of the IMFs are calculated and the results are shown in Table 1.

In Table 1, ρ_{xy} is the correlation coefficient of two IMFs, where the auto-correlation coefficient is 1, and the cross-correlation coefficients do not exceed the given threshold. And there is no mode mixing in this decomposition. The intrinsic mode function component is expressed as IMF. The decomposition results are shown in Fig. 2. And the relative error of the original component and decomposition component is shown by the red dotted line.

In Fig. 2, the decomposition components are shown by the solid blue line. It can be seen from the relative errors that the decomposition components are basically the same as the original components. Therefore, there is no frequency loss during the decomposition process. The above analysis can be shown that the noise can be removed and the effective components can be retained based on the VNCMD. However, when the practical signals are decomposed, one could not know how many signal components should be initialized. In order to further verify the effectiveness of the cross-correlation coefficient for the decomposition algorithm, the initial number of IMFs is set as 4 and the simulation signal is decomposed by

the improved VNCMD. Then, the calculated correlation coefficients are shown in Table 2.

As shown in Table 2, the maximum value of the correlation coefficients is 0.1031, which has exceeded the given threshold. Therefore, when the number of IMFs exceeds the number of the original components, the phenomena of mode mixing will be produced. This conclusion further confirms the effectiveness of the cross-correlation coefficient for the improved algorithm.

In order to reflect the advantages of the VNCMD algorithm compared with the similar algorithms, the simulation signal is decomposed by using the VMD algorithm, which is widely used in relevant researches. When the number of IMFs is set as 3, the decomposition results are shown in Fig. 3.

From Fig. 3, it can be seen that each of the components still has strong noise interference. According to the principle of VMD, it is based on the assumption of narrow-band signal decomposition. The wideband signals with overlapping frequency spectrum cannot be decomposed effectively and the fast-changing frequency components cannot be captured. At the same time, the decomposition effect will be affected by the penalty parameters and the number of IMFs. Therefore, compared with other similar algorithms, the VNCMD algorithm has a better decomposition effect on the wideband signal. And the improved VNCMD algorithm not only has the advantages of the VNCMD but also can effectively determine the number of signal components.

4 Analysis of turning machine experimental signals

## 4.1 Experimental setup for cutting chatter detection

In this section, the improved VNCMD is applied to the analysis of practical turning machine vibration signals. The vibration signals are acquired through the cutting experiment of CA6150 lathe. The experimental system is composed of a cutting tool, workpieces, vibration acceleration sensors, signal analyzers, and computers. The cutting tool material is of high-speed steel. The workpiece materials are Q235 and No. 45 steel, respectively. And ten sets of cutting experiments were performed by variable parameters on the experimental system. The cutting parameters are shown in Tables 3 and 4.

In order to acquire the more effective vibration signal during the machining process, the vibrations of different parts are studied by fixing the INV9832 vibration acceleration sensors on the front of the cutting tool and the workpiece fixture through a powerful magnetic base. The parameters of vibration acceleration sensor are shown in Table 5.

After acquiring the signal by the vibration acceleration sensors mentioned above, it is transmitted to the BK4528-B/INV3060S signal conditioner. Next, the signal is integrated

Table 1 Correlation coefficients of three IMFs

ρ_{xy}	1	2	3
1	1	0.0676	0.0832
2	0.0676	1	0.0223
3	0.0832	0.0223	1

Fig. 2 Decomposition results of simulation signal by VNCMD. **a** IMF1 and relative error in time domain. **b** IMF2 and relative error in time domain. **c** IMF3 and relative error in time domain. **d** IF and relative error with time

(a) IMF1 and relative error in time domain

(b) IMF2 and relative error in time domain

(c) IMF3 and relative error in time domain

(d) IF and relative error with time
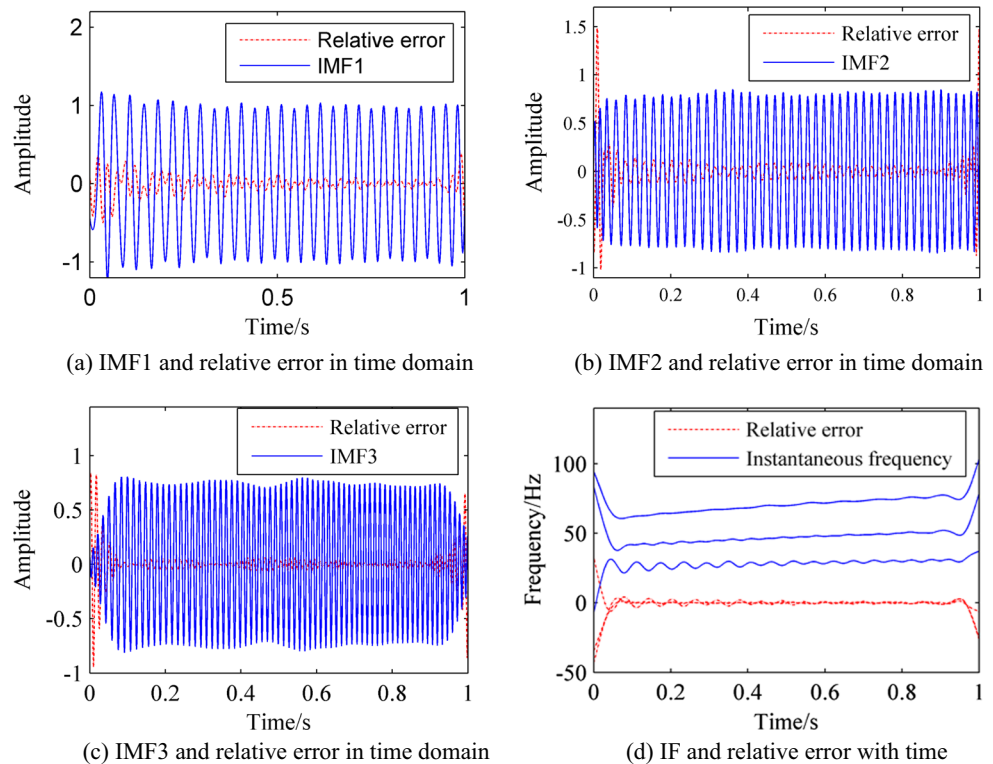
and transmitted to the computer through USB interface. The relevant signal analysis is performed by data acquisition and signal processing (DASP) software which helps us to select the appropriate vibration signal. The sampling frequency is set as 12800 Hz. The sampling time is 23 s. The experimental setup and vibration acceleration sensors are shown in Fig. 4. The execution flow of the experimental detection system is shown in Fig. 5.

As can be seen from Figs. 4 and 5, the experimental detection system has three vibration acceleration sensors. The two uniaxial vibration acceleration sensors are fixed on the workpiece fixture, and the triaxial vibration acceleration sensor is fixed on the cutting tool. Considering the limitation of paper length, the analysis of the above 10 sets of data cannot be fully displayed. Through the analysis of the vibration signals, it is found that the vibration change of the workpiece fixture is not obvious during the turning process of the machine tool. Although the vibration changes on the cutting tool are obvious, the X-axis and Z-axis directions of the sensor are susceptible to the impact of the metal chip which is not conducive

to signal analysis. Therefore, the vibration signal of the sensor of Y-axis on the cutting tool is selected as the analysis signal, where the coordinate system is machine coordinate system.

4.2 Experimental signal analysis

Through the analysis above, the third set of cutting data in Table 4 is selected as an example to analyze the cutting chatter. In order to accurately reflect the changes in the cutting process, the vibration signals for 23 s were acquired. The sampled signal in the time domain is shown in Fig. 6a, where g denotes 9.8m/s2. And the sampled signal is transformed into frequency domain by the fast Fourier transform, which is shown in Fig. 6b.

As can be seen from Fig. 6a, the cutting process is basically smooth in the former 15 s. When it reaches 16 s, the vibration amplitude begins to increase gradually, because the processing system is subjected to some kind of excitation. When it reaches 19.5 s, the vibration amplitude starts to increase sharply and may induce cutting chatter [32–34]. It can be seen from Fig. 6b that the frequency components cannot be distinguished correctly under the strong noise background. Therefore, further analysis is needed. The most obvious data of the vibration change from 18.7 to 22.3 s is extracted from the sampled signal as the target sample. The normally processed data from 1 to 5 s is extracted from the original signal as the validation sample. The waveforms of the target sample and validation sample in the time domain are shown in Fig. 7.

Table 2 Correlation coefficients of four IMFs

ρ_{xy}	1	2	3	4
1	1	0.0684	0.0911	− 0.1031
2	0.0684	1	0.0218	− 0.0145
3	0.0911	0.0218	1	0.0014
4	− 0.1031	− 0.0145	0.0014	1

Fig. 3 Decomposition results of simulation signal by VMD. **a** IMF1 and relative error in time domain. **b** IMF2 and relative error in time domain. **c** IMF3 and relative error in time domain

(a) IMF1 and relative error in time domain

(b) IMF2 and relative error in time domain

(c) IMF3 and relative error in time domain
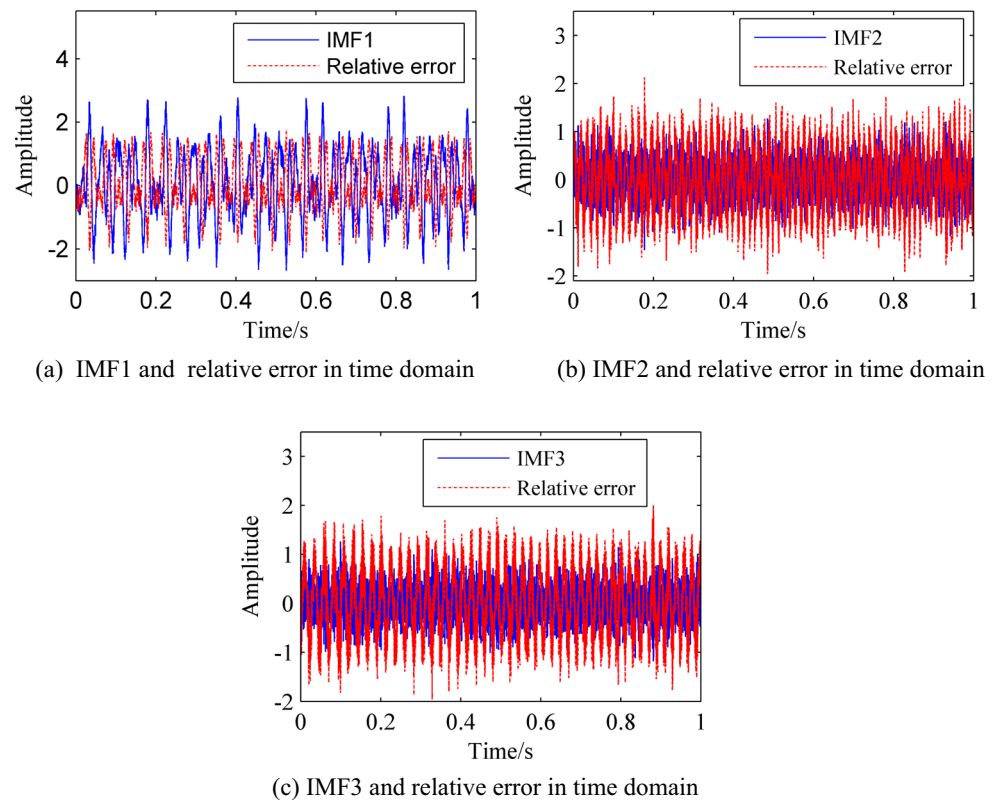
As can be seen from Fig. 7b, the target sample has distinct impulse components. It is necessary to extract the feature information from the time domain and frequency domain by signal processing method for chatter judgment. Therefore, the target sample can be analyzed by the improved VNCMD above. Considering that the impulse component is included in the target sample, an appropriate bandwidth penalty factor needs to be selected to extract the signal intrinsic mode functions. Therefore, the bandwidth penalty factor *alpha* of the time-frequency filter should be chosen to be larger, which will help the VNCMD algorithm to find correct IMFs, and the bandwidth penalty factor *beta* of the instantaneous frequency should be chosen to be smaller, which will contribute to the convergence of the VNCMD algorithm. As mentioned above, the parameters of *alpha* and *beta* should be determined by the characteristics of the signal. After several tests, the parameter *alpha* is set as 3e−3 and parameter *beta* is set as 1e−9. Calculating the correlation coefficients of the signal IMFs by the improved VNCMD

algorithm, the number of IMFs can be finally determined to be 4. And the correlation coefficients of the IMFs decomposed by the target sample are shown in Table 6. As can be seen from Table 6, the maximum correlation coefficient of the IMFs is 0.0904, which is less than the given threshold of the algorithm.

The decomposition components and Hilbert marginal spectrum of the target sample are shown in Figs. 8, 9, 10, and 11. From Fig. 8b, it can be seen that the frequency with maximum amplitude of the intrinsic mode function 1 is approximately 300 Hz. Combined with the vibration amplitude shown in Fig. 8a, it can be known that the cutting vibration of the system gradually increases, which indicates that the chatter will be generated. But the vibration energy is weak, and this weak feature is difficult to extract under strong noise background in general.

The frequency with maximum amplitude of the intrinsic mode function 2 as shown in Fig. 9b is approximately 1300 Hz. It can be concluded that this frequency is not the natural frequency of the cutting tool according to Ref. [35]. Therefore,

Table 3 Q235 steel cutting parameters

Parameter	1st	2nd	3rd	4th	5th
Rotating speed (r/min)	250	250	250	250	250
Cutting depth (mm)	0	2	3	4	5
Feed rate (mm)	0	2.7	2.7	2.7	2.7
External elongation (mm)	0	60	60	60	60
Workpiece diameter (mm)	0	50	50	50	50

Table 4 No. 45 steel cutting parameters

Parameter	1st	2nd	3rd	4th	5th
Rotating speed (r/min)	710	710	450	450	450
Cutting depth (mm)	3	5	3	6	7
Feed rate (mm)	2.7	2.7	2.7	2.7	2.7
External elongation (mm)	150	150	150	150	150
Workpiece diameter (mm)	40	40	40	40	40

Table 5 Parameters of vibration acceleration sensor

| Sensitivity	Test range	Nonlinearity	Lateral sensitivity
100 mV/g	50 g	1%	< 5%
Frequency range	Resonant frequency	Temperature range	Vibration limit
0.4–12 k (± 3 dB)Hz	40 kHz	− 50~+ 120 °C	500 g
Impact limit	Peripheral size	Weight	Output impedance
5000 g	19 × 19 × 19(mm)	12 g	< 100 Ω

Fig. 4 Experimental setup for chatter detection
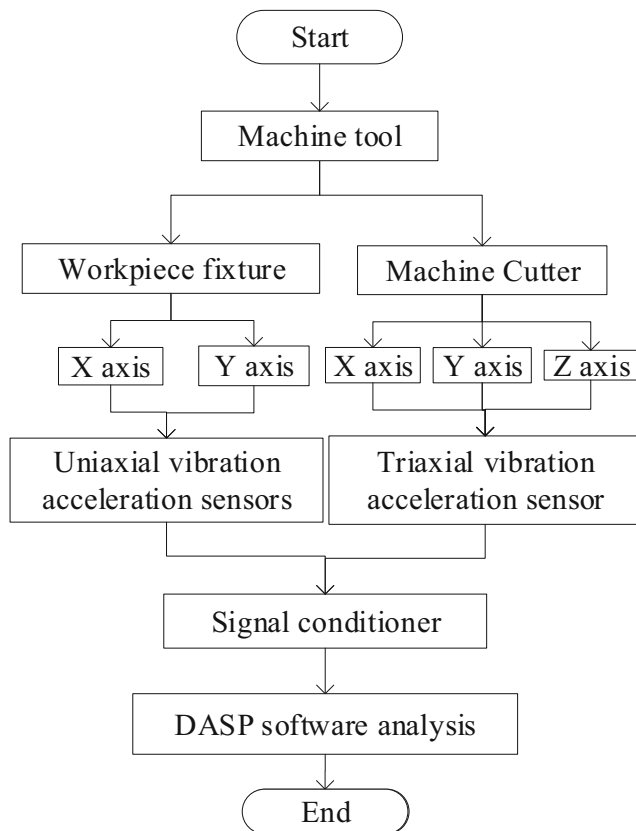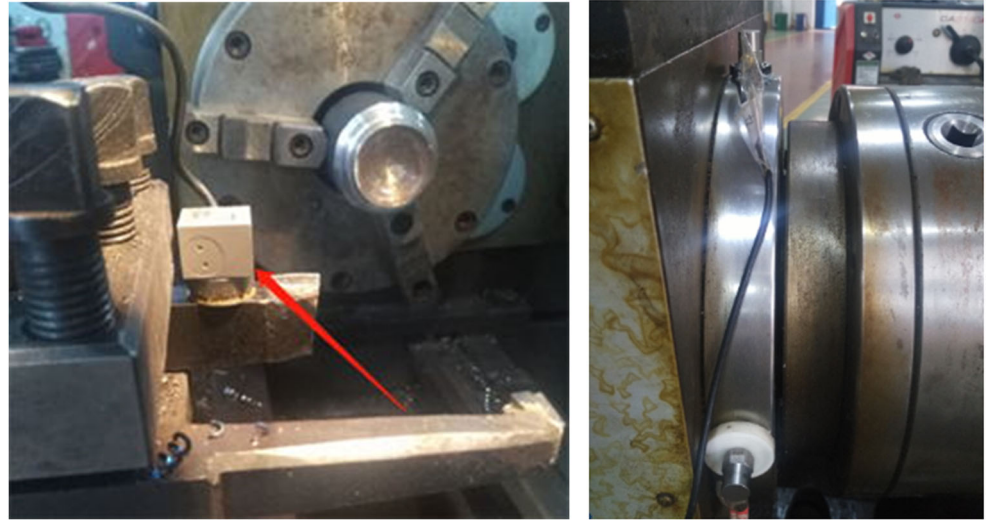
Fig. 5 Execution flow for chatter detection

the IMF2 can be considered as chatter near the natural frequency of workpiece. Combined with the vibration amplitude shown in Fig. 9a, it can be known that the vibration amplitude of IMF2 is significantly increased relative to IMF1. But the vibration energy of IMF2 does not increase significantly, which shows that the system has appeared chatter and the vibration degree is not severe. If appropriate measures can be taken, the chatter conditions can be eliminated and normal processing conditions can be restored.

The frequency with maximum amplitude of the intrinsic mode function 3 as shown in Fig. 10b is approximately 2500 Hz. According to Ref. [35], the intrinsic mode function 3 is the chatter near the natural frequency of the cutting tool. Combined with the vibration amplitude shown in Fig. 10a, the IMF3 has stronger vibration energy than IMF2, and the impulse component is produced. It shows that the cutting chatter has been induced. At this point, the cutting parameters need to be adjusted as soon as possible to avoid further development of the cutting chatter.

The frequency with maximum amplitude of the intrinsic mode function 4 as shown in Fig. 11b is approximately 3200 Hz. Combined with the vibration amplitude shown in Fig. 11a, it can be known that the IMF4 has stronger vibration energy and impulse characteristics than IMF3. It shows that the system has produced severe cutting chatter at this time. If no relevant measures are taken, there will be serious consequences.

Fig. 6 Sampled signal of chatter detection. **a** Sampled signal in the time domain. **b** Sampled signal in the frequency domain

(a) Sampled signal in time domain

(b) Sampled signal in frequency domain
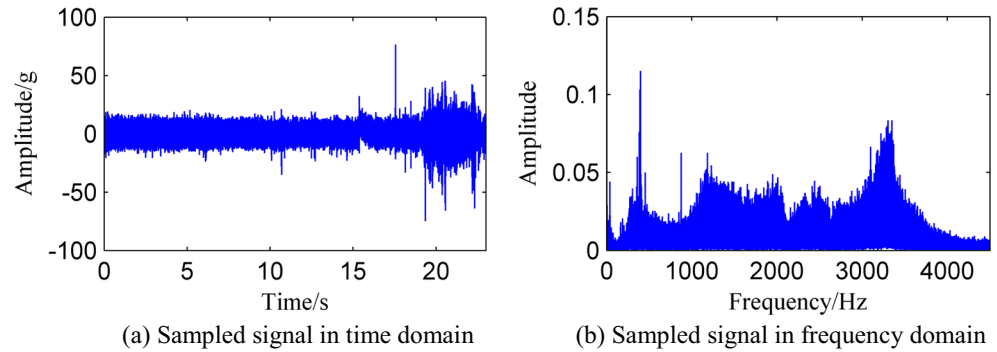
Fig. 7 Target sample in the time domain. **a** Validation sample in the time domain. **b** Target sample in the time domain

(a) Validation sample in time domain

(b) Target sample in time domain
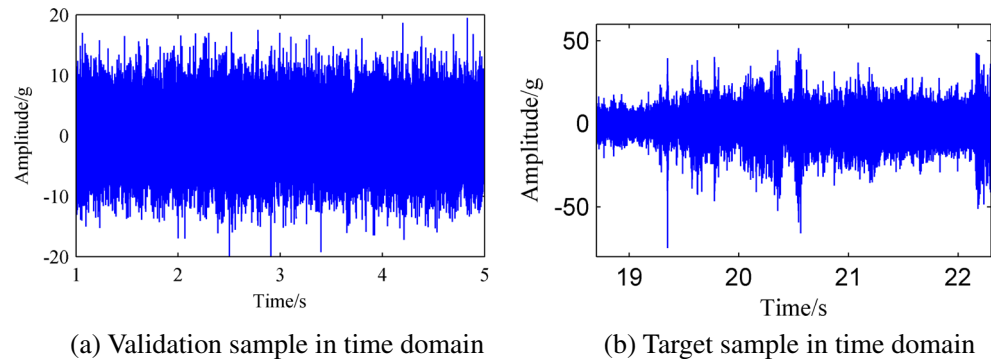
After the experiment, serious periodic scratches can be found on the left-hand side surface of the workpiece, which is shown in Fig. 12. To some extent, it reflects the consequences of cutting chatter.

Based on the above experimental analysis, it can be seen that the characteristic components of the cutting vibration signal can be effectively decomposed through the improved VNCMD, which can provide favorable conditions for subsequent feature extraction and chatter identification.

5 Chatter identification based on multi-feature vector

Although the vibration signal has been separated from the background of strong noise in the previous section, the chatter stages are still difficult to distinguish. In the machining process, two issues of cutting chatter that need to be

**Table 6** Correlation coefficients of four IMFs in the target sample

ρ_{xy}	1	2	3	4
1	1	0.0030	0.0904	0.0048
2	0.0030	1	0.0037	0.0724
3	0.0904	0.0037	1	0.0508
4	0.0048	0.0724	0.0508	1

concerned are whether or not the chatter has occurred and at what extent the chatter has developed. To accurately identify whether the cutting chatter is generated, it is necessary to extract chatter features from the time domain and frequency domain of the intrinsic mode functions to obtain feature vectors by using relevant statistical methods. Therefore, the fourth-order cumulant and permutation entropy are used to extract the features from the target sample and validation sample of the experimental signal [36, 37]. The fourth-order cumulant can suppress the influence of Gauss noise and characterize the nonlinearity of signals. Compared with low-order cumulant, more information of signals can be obtained from the fourth-order cumulant. And permutation entropy can be used to detect the qualitative and quantitative dynamic changes in time series [38]. It has a good effect on the detection of impulse components and has a strong anti-noise ability. This combined eigenvector cannot only extract useful information from abrupt and strong interfering signals but also eliminate the interference caused by unexpected factors.

The fourth-order cumulants and permutation entropies of the target sample and validation sample are shown in Fig. 13, where the target sample and validation sample represent the machining with chatter and normal machining, respectively. Each of the statistical points represents the fourth-order cumulant of the target sample and the validation sample for 10,000 data points as shown in
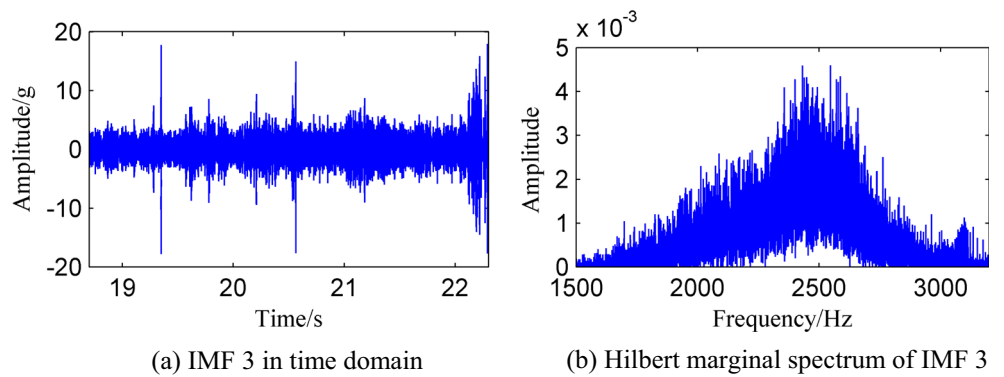
Fig. 8 Intrinsic mode function 1 of the target sample. **a** IMF1 in the time domain. **b** Hilbert marginal spectrum of IMF1

(a) IMF1 in time domain

(b) Hilbert marginal spectrum of IMF1
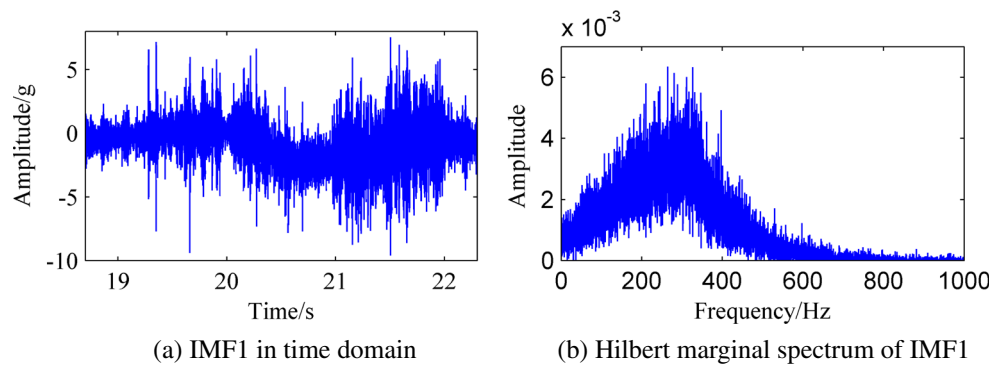
Fig. 9 Intrinsic mode function 2 of the target sample. **a** IMF2 in the time domain. **b** Hilbert marginal spectrum of IMF2

(a) IMF 2 in time domain

(b) Hilbert marginal spectrum of IMF2
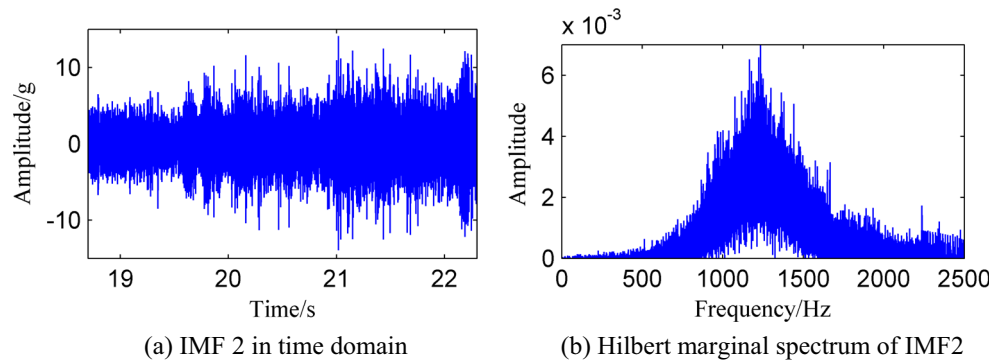
Fig. 10 Intrinsic mode function 3 of the target sample. **a** IMF3 in the time domain. **b** Hilbert marginal spectrum of IMF3

(a) IMF 3 in time domain

(b) Hilbert marginal spectrum of IMF 3

Fig. 11 Intrinsic mode function 4 of the target sample. **a** IMF4 in the time domain. **b** Hilbert marginal spectrum of IMF4

(a) IMF 4 in time domain
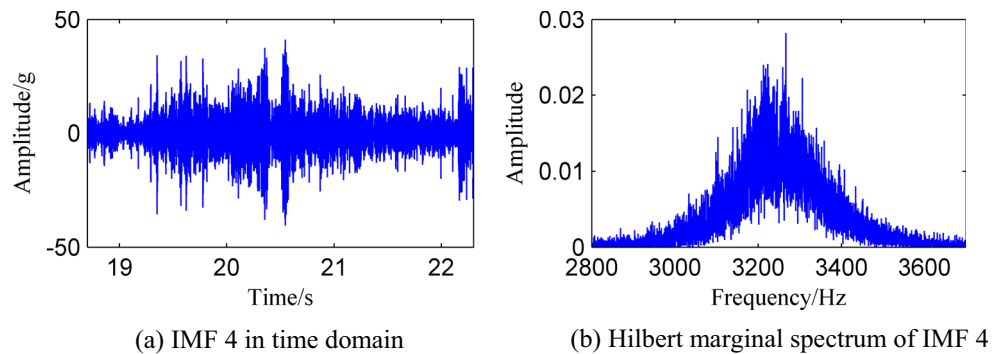
(b) Hilbert marginal spectrum of IMF 4

Fig. 12 Workpiece after machining

Fig. 13a, which can reflect the degree of deviation of signal from Gaussian distribution. And each of the statistical points represents the permutation entropy of the tar-

get sample and validation sample for 1,452 data points as shown in Fig. 13b, which can reflect the impulse component in the signal. As can be seen from Fig. 13a, there are obvious differences between these two statuses, which can be used as a criterion for the occurrence of chatter. The fourth-order cumulant of the validation sample is smooth, which indicates that the cutting process is normal. The fourth-order cumulant of target sample increases gradually at first then appears three peak values, and then it decreases slightly at last. It shows that the weak cutting chatter occurs at the beginning, and three types of severe cutting chatter may occur with the increase of cutting chatter degree. In Fig. 13b, the features cannot be distinguished from the two statuses because of the aliasing from 7 to 14 points.

Fig. 13 Features of samples. **a** Fourth-order cumulants of the samples. **b** Permutation entropies of the samples

(a) Fourth-order cumulants of samples
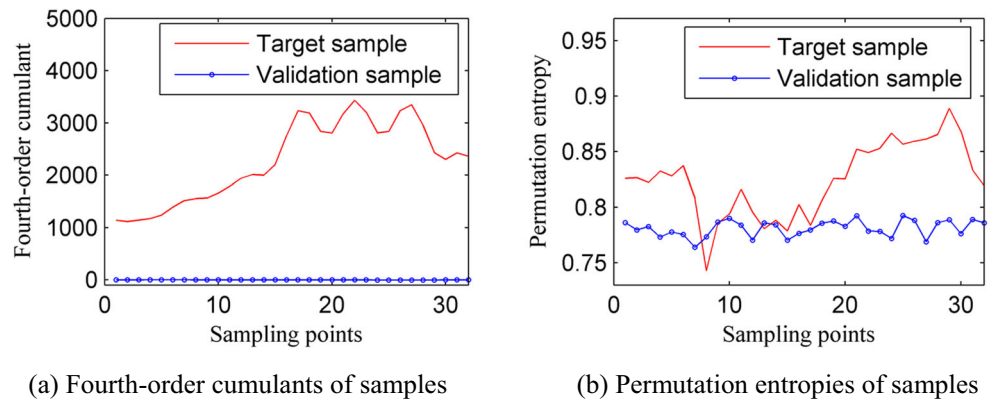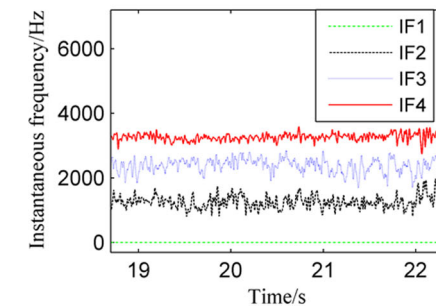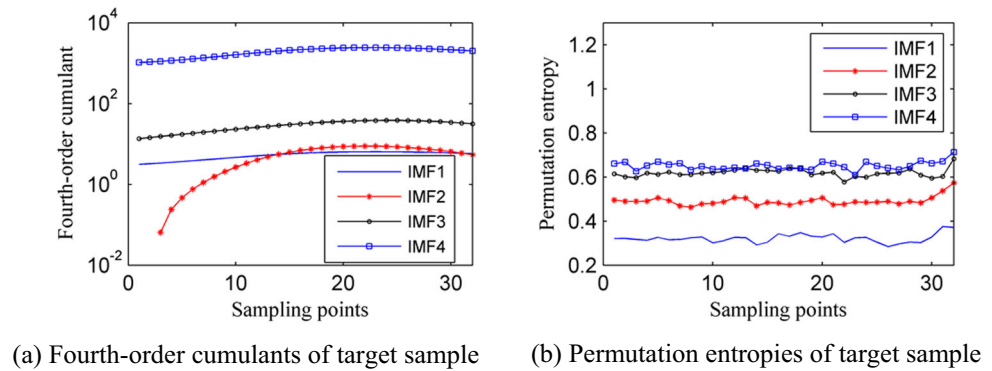
(b) Permutation entropies of samples

Fig. 14 Multi-feature vector of the target sample. **a** Fourth-order cumulants of the target sample. **b** Permutation entropies of the target sample. **c** Instantaneous frequencies of the target sample

(a) Fourth-order cumulants of target sample

(b) Permutation entropies of target sample

(c) Instantaneous frequencies of the target sample

When the cutting chatter occurs, the type and extent of chatter development need to be further identified. The target sample is decomposed into several components by the improved VNCMD. And the fourth-order cumulants, permutation entropies, and instantaneous frequencies of each component can be obtained, which are shown in Fig. 14.

The four decomposition components represent the four stages of chatter development. Combined with the Hilbert marginal spectrum analysis results in Figs. 8, 9, 10, and 11, it can be known that IMF1 denotes the initial stage of chatter, IMF2 denotes the chatter near the natural frequency of workpiece, IMF3 denotes the chatter near the natural frequency of the cutting tool, and IMF4 denotes the sharp development of chatter. It can be seen from Fig. 14a that the features of IMF1 and IMF2 are overlapped and the features of IMF3 and IMF4 can be distinguished clearly. In Fig. 14b, the permutation entropies of IMF1 and IMF2 can be distinguished clearly, but the permutation entropies of IMF3 and IMF4 are very close, which are not conducive to the judgment of the cutting chatter status. It can be seen from Fig. 14c that the type and extent of chatter development can be distinguished clearly by the instantaneous frequencies of the four intrinsic mode functions of the target sample. Therefore, if these three characteristics are considered comprehensively, it will be more helpful to identify the type and extent of cutting chatter. The above analysis indicates that the multi-feature vector is more accurate to identify the development of chatter.

6 Conclusions

Aiming at the problem that the vibration signal of turning process is susceptible to noise interference and low signal-to-noise ratio, a cutting chatter identification method based on the improved VNCMD and multi-feature vector is proposed in this paper. The improved VNCMD algorithm not only has the advantages of the original VNCMD algorithm but also can accurately determine the number of signal components. Compared with the ordinary narrow-band signal decomposition algorithm, this improved algorithm can effectively eliminate the noise interference and extract the characteristic components of the signal. Through the analysis results of the multi-feature vector of the cutting vibration signal, it can be seen that this method has good weak feature extraction ability and can greatly improve the accuracy of the cutting chatter identification. The good classification results also indicate that the multi-feature vector is suitable to chatter status recognition.

For future work, although the multi-feature vector based on the improved VNCMD algorithm has a good performance, this method might not be the optimal choice. How to choose and estimate the feature vector is still a challenge work for pattern recognition. Therefore, the intelligent identification of cutting chatter based on the feature vectors is our next step work.

References

1. Smith S, Tlusty J (1997) Current trends in high-speed machining. ASME J Manuf Sci Eng 119(4):664–666. https://doi.org/10.1115/1.2836806
2. Ji YJ, Wang XB, Liu ZB, Wang HJ, Jiao L, Zhang L, Huang T (2018) Milling stability prediction with simultaneously considering the multiple factors coupling effects-regenerative effect, mode coupling, and process damping. Int J Adv Manuf Technol 97(5–8):2509–2527. https://doi.org/10.1007/s00170-018-2017-7
3. Weremczuk A, Rusinek R (2016) Influence of frictional mechanism on chatter vibrations in the cutting process–analytical approach. Int J Adv Manuf Technol 89(9):12):1–12):8. https://doi.org/10.1007/s00170-016-9520-5
4. Zhang XJ, Xiong CH, Ding Y, Feng MJ, Xiong YL (2012) Milling stability analysis with simultaneously considering the structural mode coupling effect and regenerative effect. Int J Mach Tool Manu 53(1):127–140. https://doi.org/10.1016/j.ijmachtools.2011.10.004
5. Yan Y, Xu J, Wiercigroch M (2017) Regenerative chatter in a plunge grinding process with workpiece imbalance. Int J Adv Manuf Technol 89(9–12):2845–2862. https://doi.org/10.1007/s00170-016-9830-7
6. Yan Y, Xu J, Wiercigroch M (2018) Stability and dynamics of parallel plunge grinding. Int J Adv Manuf Technol 99(1–4):881–895. https://doi.org/10.1007/s00170-018-2440-9
7. Kim JS, Lee BH (1991) An analytical model of dynamic cutting forces in chatter vibration. Int J Mach Tool Manu 31(3):371–381. https://doi.org/10.1016/0890-6955(91)90082-E
8. Zhang HT, Wu Y, He DF, Zhao H (2015) Model predictive control to mitigate chatters in milling processes with input constraints. Int J Mach Tool Manu 91:54–61. https://doi.org/10.1016/j.ijmachtools.2015.01.002
9. Shorr MJ, Liang SY (1996) Chatter stability analysis for end milling via convolution modelling. Int J Adv Manuf Technol 11(5):311–318. https://doi.org/10.1007/BF01845689
10. Chen CK, Tsao YM (2006) A stability analysis of turning a tailstock supported flexible work-piece. Int J Mach Tool Manu 46(1):18–25. https://doi.org/10.1016/j.ijmachtools.2005.04.002
11. Choi T, Shin YC (2003) On-line chatter detection using wavelet-based parameter estimation. J Manuf Sci Eng 125(1):21–28. https://doi.org/10.1115/1.1531113
12. Wu Y, Du R (1996) Feature extraction and assessment using wavelet packets for monitoring of machining processes. Mech Syst Signal Process 10(1):29–53. https://doi.org/10.1006/mssp.1996.0003
13. Vela-Martínez L, Jauregui-Correa JC, Rodriguez E, Alvarez-Ramirez J (2010) Using detrended fluctuation analysis to monitor chattering in cutter tool machines. Int J Mach Tool Manu 50(7):651–657. https://doi.org/10.1016/j.ijmachtools.2010.03.012
14. Kuljani E, Sortino M, Totis G (2008) Multisensor approaches for chatter detection in milling. J Sound Vib 312(4–5):672–693. https://doi.org/10.1016/j.jsv.2007.11.006
15. Kuljanic E, Totis G, Sortino M (2009) Development of an intelligent multisensor chatter detection system in milling. Mech Syst Signal Process 23(5):1704–1718. https://doi.org/10.1016/j.ymssp.2009.01.003
16. Liu CF, Zhu LD, Ni CB (2017) The chatter identification in end milling based on combining EMD and WPD. Int J Adv Manuf

Technol 91(9–12):3339–3348. https://doi.org/10.1007/s00170-017-0024-8

17. Ji YJ, Wang XB, Liu ZB, Yan ZG, Li J, Wang DQ, Wang JQ (2017) EEMD-based online milling chatter detection by fractal dimension and power spectral entropy. Int J Adv Manuf Technol 92(1–4): 1185–1200. https://doi.org/10.1007/s00170-017-0183-7

18. Cao HR, Zhou K, Chen XF (2015) Chatter identification in end milling process based on EEMD and nonlinear dimensionless indicators. Int J Mach Tools Manuf 92:52–59. https://doi.org/10.1016/j.ijmachtools.2015.03.002

19. Wang YX, Markert R, Xiang J, Zheng WG (2015) Research on variational mode decomposition and its application in detecting rub-impact fault of the rotor system. Mech Syst Signal Process 60–61:243–251. https://doi.org/10.1016/j.ymssp.2015.02.020

20. Chen SQ, Dong XJ, Peng ZK, Zhang WM (2017) Nonlinear chirp mode decomposition: a variational method. IEEE Trans Signal Process 65(22):6024–6037. https://doi.org/10.1109/TSP.2017.2731300

21. Grabec I, Gradišek J, Govekar E (1999) A new method for chatter detection in turning. CIRP Ann- Manuf Technol 48(1):29–32. https://doi.org/10.1016/s0007-8506(07)63125-4

22. Berger B, Belai C, Anand D (2003) Chatter identification with mutual information. J Sound Vib 267(1):178–186. https://doi.org/10.1016/s0022-460x(03)00067-1

23. Tansel IN, Li M, Demetgul M, Bickraj B, Ozcelik B (2012) Detecting chatter and estimating wear from the torque of end milling signals by using index based reasoner (IBR). Int J Adv Manuf Technol 58(1–4):109–118. https://doi.org/10.1007/s00170-010-2838-5

24. Cao HR, Lei YG, He ZG (2015) Chatter identification in end milling process using wavelet packets and Hilbert-Huang transform. Int J Mach Tools Manuf 92:52–59. https://doi.org/10.1016/j.ijmachtools.2013.02.007

25. Kowalski M, Meynard A, Hua-tieng W (2016) Convex Optimization approach to signals with fast varying instantaneous frequency. Appl Comput Harmon Anal 9(9):1260–1267. https://doi.org/10.1016/j.acha.2016.03.008

26. Dragomiretskiy K, Zosso D (2014) Variational mode decomposition. IEEE Trans Signal Process 62(3):531–544. https://doi.org/10.1109/TSP.2013.2288675

27. Carson JR (1922) Notes on the theory of modulation. 10(1):57–64. https://doi.org/10.1109/proc.1963.2322

28. Meignen S, Pham DH, Mclaughlin S (2017) On demodulation, ridge detection, and synchrosqueezing for multicomponent signals. IEEE Trans Signal Process 65(8):2093–2103. https://doi.org/10.1109/TSP.2017.2656838

29. Pan MC, Lin YF (2006) Further exploration of Vold–Kalman-filtering order tracking with shaft-speed information—II: engineering applications. Mech Syst Signal Process 20(6):1410–1428. https://doi.org/10.1016/j.ymssp.2005.01.007

30. Auger F, Flandrin P (1995) Improving the readability of time-frequency and time-scale representations by the reassignment method. IEEE Transactions on Signal Processing 43(5):1068–1089. https://doi.org/10.1109/78.382394

31. Ahlgren P, Jarneving B, Rousseau R (2003) Requirements for a cocitation similarity measure, with special reference to Pearson's correlation coefficient. J Am Soc Inf Sci Technol 54(6):550–560. https://doi.org/10.1002/asi.10242

32. Balachandran B (2001) Nonlinear dynamics of milling processes. Philos Trans R Soc A Math Phys Eng Sci 359(1781):793–819. https://doi.org/10.1098/rsta.2000.0755

33. Gilsinn DE, Davies MA, Balachandran B (2001) Stability of precision diamond turning processes that use round nosed tools. J Manuf Sci Eng 123(4):747. https://doi.org/10.1115/1.1373648

34. Balachandran B, Gilsinn D (2005) Non-linear oscillations of milling. Math Comput Model Dyn Syst 11(3):273–290. https://doi.org/10.1080/13873950500076479

35. Sekar M, Srinivas J, Kotaiah KR, Yang SH (2009) Stability analysis of turning process with tailstock-supported workpiece. Int J Adv Manuf Technol 43(9–10):862–871. https://doi.org/10.1007/s00170-008-1764-2

36. Lyu S, Farid H (2003) Detecting hidden messages using higher-order statistics and support vector machines. In: Petitcolas FAP (ed) Information hiding. IH 2002. Lecture Notes in Computer Science, vol 2578. Springer, Berlin, Heidelberg. https://doi.org/10.1007/3-540-36415-3_22

37. Bandt C, Pompe B (2002) Permutation entropy: a natural complexity measure for time series. Phys Rev Lett 88(17):174102. https://doi.org/10.1103/PhysRevLett.88.174102

38. Cao Y, Tung WW, Gao JB, Protopopescu VA, Hively LM (2004) Detecting dynamical changes in time series using the permutation entropy. Phys Rev E 70(4 Pt 2):046217. https://doi.org/10.1103/PhysRevE.70.046217